J Solid State Electrochem (2014) 18:1665–1671
DOI 10.1007/s10008-014-2401-7

ORIGINAL PAPER

Effect of pore size/distribution in TiO_2 films on agarose gel electrolyte-based dye-sensitized solar cells

Hsin-Ling Hsu · Cheng-Fang Tien · Jihperng Leu

Received: 16 September 2013 / Revised: 14 January 2014 / Accepted: 20 January 2014 / Published online: 7 February 2014

Abstract This study develops a simple method to change the distribution of the pore size in a TiO_2 layer, using polyethylene glycol (PEG), while maintaining nearly the same surface area and porosity to clarify how large pores affect the performance of dye-sensitized solar cells (DSSCs). Specifically, a heating step at 100 °C for a specific duration is added prior to PEG removal and TiO_2 sintering at 400 °C. This process transforms the role of the PEG from a surfactant to a pore generator (porogen) and forms larger pores, depending on the loading and aggregation time for the PEG to gain larger pores. The effect of larger pores in TiO_2 films under 30 % PEG loading, on the performance of an agarose gel electrolyte-based DSSC, was further investigated using the ionic liquid, 1-allyl-3-ethylimidazolium iodide (AEII). The *I–V* characteristic and the electrochemical impedance spectroscopy analysis show that larger pores readily improve redox couple diffusion in a TiO_2 porous electrode and modify the interface between electrolyte and TiO_2. Using the optimized TiO_2 film with larger pores (30 % PEG loading, 100 °C/60 min), an efficiency of 7.43 % is achieved for the agarose gel electrolyte-based DSSC, which represents a 26.1 % improvement over TiO_2 without the addition of PEG.

Keywords Dye-sensitized solar cell · Pore size distribution · Polyethylene glycol · Agarose gel · Ionic liquids

Electronic supplementary material The online version of this article (doi:10.1007/s10008-014-2401-7) contains supplementary material, which is available to authorized users.

H.-L. Hsu · C.-F. Tien · J. Leu (✉)
Department of Materials Science and Engineering, National Chiao Tung University, 1001 University Road, Hsinchu, Taiwan 30010
e-mail: jimleu@mail.nctu.edu.tw

Introduction

In recent years, dye-sensitized solar cells (DSSCs) have been the subject of much scientific research and have found many industrial applications, because of their high efficiency, simple fabrication process, and low cost [1]. In 2011, a photo-to-electricity conversion efficiency of 12.3 % was achieved and reported [2]. DSSCs are expected to become a viable alternate to conventional silicon solar cells.

To date, extensive research involving DSSCs has focused on the key constituents, such as the semiconductor electrode [3–5], the dye [6–8], the electrolyte [9–11], and the counter electrode [12, 13], to improve the performance of DSSCs. Specifically, liquid electrolyte loss caused by leakage and volatilization has been one of the major problems limiting the long-term use of DSSC. Gel and solid state electrolytes are the viable solutions to make the sealing process easier and to minimize the loss of electrolytes for enhanced durability [10, 14]. When gel or solid electrolyte is introduced in DSSCs for enhanced cell durability, the pore morphology of TiO_2 films is even more critical because the viscous and steric effects of the gel or solid electrolytes make it especially difficult to fill the porous TiO_2 films completely [14, 15]. Moreover, it is found that large pores result in a higher electron lifetime in the TiO_2 electrode [16]. The pore morphology, which involves the pore size/distribution, surface area, and the porosity, of the porous films utilized in fuel cell [17] and lithium air battery [18], has great impact on their performance. Similarly, the pore morphology of a TiO_2 film also greatly influences the efficiency of a DSSC [19]. To date, the pore morphology of TiO_2 film has been modified by using (1) porogens, such as ethyl cellulose [20], [poly(ethylene oxide)$_{106}$-poly-(propylene oxide)$_{70}$-poly-ethylene oxide)$_{106}$] (Pluronic® F127) [21] and poly(methyl methacrylate) (PMMA) [22] with different molecular weights and loadings, (2) binders such as polyethylene glycol (PEG) under various loadings [23] and molecular weights [24], and

(3) different TiO_2 particle sizes [16, 25]. However, in modifying the TiO_2 particle size, the loading and molecular weight of any binders or porogen can simultaneously change the surface area, porosity, and pore size. This makes it difficult to quantitatively analyze the impact of pore morphology (surface area, porosity, and pore size/distribution) on DSSC performance.

This study develops a simple method to control the distribution of the pore size in the TiO_2 layer, using polyethylene glycol as the porogen, while maintaining the surface area and porosity. Specifically, a heating step at 100 °C for a specific duration is added prior to PEG removal and TiO_2 sintering at 400 °C, to modulate the pore morphology. The effects of the PEG loadings and isothermal heating time on the pore morphology (pore size/distribution, porosity, and surface area) are firstly investigated. The correlation between the pore size/distribution and the DSSCs performance is then examined, using agarose gel electrolyte and the ionic liquid, 1-allyl-3-ethylimidazolium iodide (AEII) [26, 27]. In addition, the pore properties, the photocurrent vs. voltage (*I–V*) curve, and the AC impedance are measured and analyzed, in order to determine the factors that affect the conversion efficiency of DSSCs.

Experimental

Titanium dioxide (25 nm, anatase phase) and poly(ethylene glycol) (PEG; molecular weight=100,000 g/mol) were purchased from Sigma Aldrich. N719 (ruthenium 535-bis TBA) was procured from Uni-Region Biotech. Guanidinium thiocyanate (99 %) (GuSCN), N-methylbenzimidazole (99 %) (NMBI), and 3-methoxypropionirile (MPN) were obtained from Alfa Aesar. Lithium iodide (LiI) was purchased from Merck. Titanium tetrachloride ($TiCl_4$) was purchased from Showa Chemicals. Glass substrates coated with a fluorine-doped tin-oxide (FTO) layer, with a sheet resistance of 8Ω/ϒ, were obtained from Hartford Glass Co. All chemicals were used as received, without further purification, unless otherwise stated. The synthesis procedure for AEII followed a previously reported methodology [28].

PEG was added to de-ionized water (4.5 g) in a specific ratio relative to the weight of TiO_2. The solution was then stirred for 1 h. Anatase TiO_2 nanopowder (0.9 g) was then added to the PEG/water solution and stirred for another 48 h. The FTO-coated glass was cleaned with acetone and ethanol, prior to use. The nano-crystalline TiO_2 thin film (~10-μm thickness) was coated onto the FTO glass using the doctor-blading technique and then dried under vacuum. The as-prepared TiO_2 films were dried in air and then heated at 100 °C on a hot plate, for a specific duration, to allow the aggregation of PEG, in order to modulate the PEG size/distribution inside the TiO_2 matrix. Finally, the porous TiO_2 thin films were formed by removing PEG and sintering at 400 °C for 30 min.

The N_2 gas adsorption–desorption curves for the TiO_2 films were plotted using a NOVA 1000e Surface Area Analyzer (Quantachrome instrument, USA). The specific surface area was determined from the linear portion of Brunauer–Emmet–Teller (BET) equation (P/P^0=0.05–0.30). The pore size distribution was calculated using a non-local density functional theory (NLDFT) model [29]. The film thickness was measured using a field-emission scanning electronic microscope (FE-SEM), JSM-6700F (JOEL, Japan).

The solution for the scattering layer was produced by adding TiO_2 anatase nanopowder of 400-nm diameter (0.4 g, ECOH) and poly(ethylene glycol)-block-poly(propylene glycol)-block-poly(ethylene glycol) (P123) (0.5 g, Sigma Aldrich) into n-butanol (4 g) and stirring well. Subsequently, a 4-μm-thick scattering layer was deposited by spin-coating onto the sintered TiO_2 working layer, followed by sintering at 400 °C for 30 min. The dual-TiO_2-layer (scattering TiO_2 on working TiO_2 electrode) was immersed in an aqueous 0.1 M $TiCl_4$ solution for 30 min, using an ice bath. The dual-TiO_2-layer was then annealed at 450 °C for 1 h, to ensure excellent binding between the TiO_2 particles and the conversion of any remaining amorphous TiO_2 to anatase phase. Finally, the FTO/TiO_2 photo-anode was sensitized in a N719 dye/ethanol solution (3×10^{-4} M) at room temperature for 24 h. The DSSC cell was fabricated by sealing the dye-sensitized TiO_2 photo-anode and a Pt-sputtered cathode at approximately 100 °C, using a 25-μm hot-melt sealing foil (SX1170-25, SOLARONIX), which also served as a spacer. The agarose gel electrolyte consisted of 1.5 M AEII, 0.1 M GuSCN, 0.2 M NMBI, 0.05 M I_2, and 0.5 wt% agarose in low toxicity PC/DMSO co-solvents (volume ratio, 8:2). A DSSC cell (active area: 0.28 cm^2) was produced upon the injection of the gel agarose electrolyte into the cell. Ionic liquid AEII-based agarose gel electrolyte was selected because its performance is comparable to MPN-based (3-methoxypropionirile) liquid electrolyte [30].

An AM1.5G Solar Simulator (Newport 3A) was used as a light source, with the incident light at 100 mW cm^{-2}, and calibrated using a standard Si solar cell (ORIEL), to evaluate the photocurrent conversion efficiency. The conversion efficiency was calculated from the photocurrent vs. voltage (*I–V*) curve, which was measured using a Keithley 2,400 source meter. The impedances between the interfaces inside the DSSC were measured by electrochemical impedance spectroscopy (EIS) and are shown in Nyquist plots. The EIS measurements were performed using a potentiostat/galvanostat (PGSTAT100; Autolab) over the frequency range from 0.01 to 10^6 Hz, with an amplitude of 10 mV. All measurements in this study were performed at 25 °C.

Results and discussion

The distribution of the pore size in the TiO_2 films prepared using various PEG loadings, with direct sintering at 400 °C, was firstly examined. Using direct sintering at 400 °C for 0.5 h, the pore size distributions, based on a NLDFT model, of the porous TiO_2 films prepared using different PEG loadings are shown in Fig. 1a. When PEG is added to the TiO_2 film, the peak pore size shifts slightly from ~18 nm (no PEG) to 22–25 nm, for PEG loadings ranging from 20 to 100 %. A peak pore size of ~36 nm results from a PEG loading ≥40 %. The relative percentage of the 36-nm peak increases as the PEG loading increases up to 80 %, then drops slightly at a 100 % PEG loading. In short, when there is PEG loading of the TiO_2 at less than 40 %, the pore size distributions are slightly increased over those of TiO_2 films without PEG addition. These pores are mainly constructed from the crevices of the TiO_2 particle crevices. In the TiO_2 nanoparticle/PEG paste, PEG acts as a surfactant and is coated onto the TiO_2 nanoparticle surface via hydrogen bonding, which inhibits the aggregation of nanoparticles [31]. Little extra volume is occupied by the PEG in the TiO_2 thin film, prior to burning out at 400 °C. When the PEG loading is ≥40 %, the pore size is larger (~36 nm) and its relative percentage increases with PEG loadings. This indicates that in the TiO_2 nanoparticle/PEG paste, PEG is not only coated onto the TiO_2 nanoparticles but also occupies extra volume. Therefore, PEG serves as a porogen [28], which is transformed into additional larger pores after PEG burn-out. As the PEG loading increases, the amount of larger pores increases, as demonstrated by the increased peak height at ~36 nm.

The surface areas and porosity of the TiO_2 films are summarized in Table 1. The surface area is mainly controlled by the size of the TiO_2 nanoparticles. Without PEG, the surface area of the TiO_2 film is 50.15 $m^2\ g^{-1}$, in this study, which is close to the published data, 53 $m^2\ g^{-1}$ [32]. The surface area and porosity are slightly reduced to ~49 $m^2\ g^{-1}$, when the PEG loading is raised to less than 40 %, presumably due to a slightly larger distribution of pore size and insufficient packing under direct sintering. At a PEG loading ≥40 %, but less than 80 %, surface area and porosity reach 50.50–51.75 $m^2\ g^{-1}$ and 49.6–51.1 %, respectively. At 80 % loading and above, while the surface area remains at approximately 50.93 $m^2\ g^{-1}$, the porosity decreases from 50.52 to 47.46 %, due to film collapse, namely, the decrease in the film thickness, from 10 to 6 μm, after PEG burn-out.

The rheological behavior of PEG as a function of temperature was then determined (supporting data, Appendix 1). The viscosity of PEG ($T_{melting}$=60 °C) drops significantly from 1.1×10^6 poises to nearly 8×10^4 at $T\geq65$ °C, so the mobility is substantially enhanced. An isothermal heating step at 100 °C was thus added to control the pore morphology of the TiO_2 films by taking advantage of the PEG's high mobility and ability to aggregate, without decomposition. Figure 1b illustrates the pore size distribution of TiO_2 films with various initial PEG loadings, prepared using an additional heating step at 100 °C for 1 h and then sintering at 400 °C for 0.5 h. The pore size distribution of the TiO_2 film with 0 % PEG loading is not obviously different to that with an intermediate heating step at 100 °C. When the loading is increased to 30 %, larger mesopores (~36 nm) are formed with the additional heating step. When the PEG loading is 40 % or higher, the amount of larger mesopores (~36 nm) increases and macropores with a diameter >50 nm also appear.

After the aggregation process for a PEG loading ≤40 %, the surface areas of the TiO_2 films decreases a little, but still

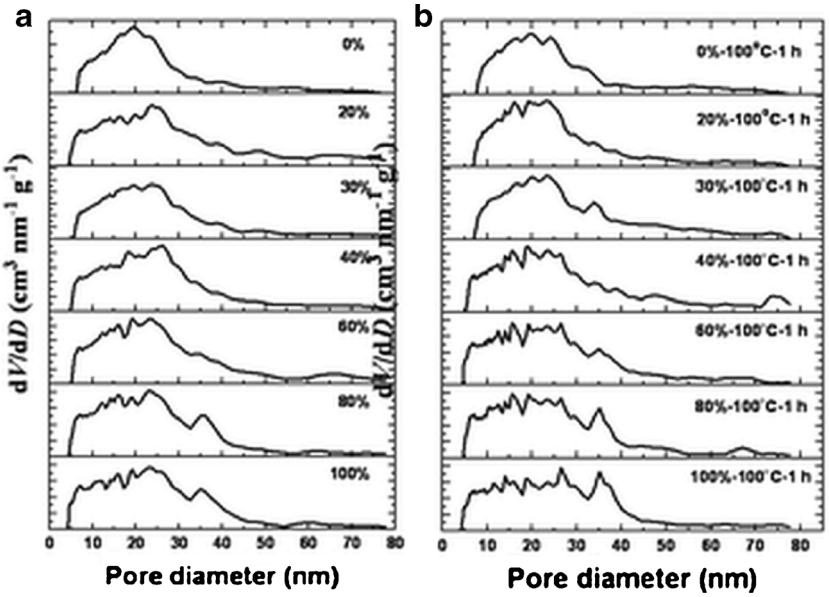

Fig. 1 The pore size distribution of TiO_2 layer under different PEG loadings (20–100 % relative to TiO_2 weight) based on NLDFT model: **a** sintered at 400 °C for 0.5 h directly and **b** kept at 100 °C for 1 h, then sintered at 400 °C for 0.5 h

Table 1 The surface area and porosity in TiO_2 thin films prepared by using various PEG loadings with different sintering processes

Heating condition	Sample properties	0 %	20 %	30 %	40 %	60 %	80 %	100 %
Direct 400 °C sintering for 0.5 h	Surface area (m^2 g^{-1})	50.15	48.97	49.27	50.85	51.75	50.93	51.57
	Porosity (%)	52.35	50.62	49.64	51.14	50.52	47.46	47.13
100 °C/1 h, then 400 °C/0.5 h	Surface area (m^2 g^{-1})	48.20	48.45	48.90	49.77	49.99	51.14	49.06
	Porosity (%)	52.33	51.32	53.99	54.28	47.19	47.46	46.97

remains around 50 m^2 g^{-1}, as listed in Table 1. Meanwhile, the porosity increases slightly, compared with the TiO_2 films prepared by direct burn-out at 400 °C. However, when PEG loading is ≥60 %, the porosity decreases, similar to the case for ≥80 % PEG loading with a direct sintering process. The PEG aggregation deteriorates the structural integrity of the TiO_2 films and causes the film to collapse at PEG loadings, ≥60 %, which phenomenon is not evident for loadings ≥80 % with direct sintering. The results confirm that larger pores are introduced readily through PEG aggregation at 100 °C, because of the enhanced diffusivity at a reduced viscosity, as described by the kinetic molecular theory of Brownian motion, based on the Einstein–Stokes equation [33, 34]. With higher PEG loadings (≥60 %), macropores with a diameter >50 nm and interconnected pores weaken the skeleton of the TiO_2 and cause the film to collapse.

In addition to PEG loadings, isothermal heating time is another factor that controls pore morphology through the extent of PEG aggregation. A 30 % PEG loading was selected in this study to determine the effect of heating time (0–150 min) at 100 °C on the pore size distribution in the TiO_2 films, as illustrated in Fig. 2, because this loading provides enough PEG to modulate the pore morphology via PEG aggregation at 100 °C, but avoids serious film shrinkage. Meanwhile, the images of SEM of these TiO_2 films showed no obvious difference in surface morphology (supporting data, Appendix 2). From Fig. 2, there is a peak pore size of ~32 nm, due to PEG aggregation into the larger pores, after heating at 100 °C for 30 min. At 100 °C, the interaction

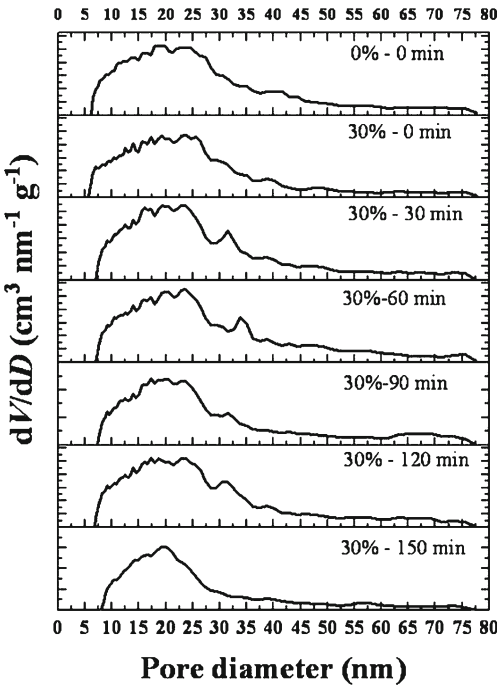

Fig. 2 The pore size distributions of TiO_2 layer at 30 % PEG loadings based on NLDFT model: various isothermal heating time at 100 °C, followed by sintering at 400 °C/0.5 h

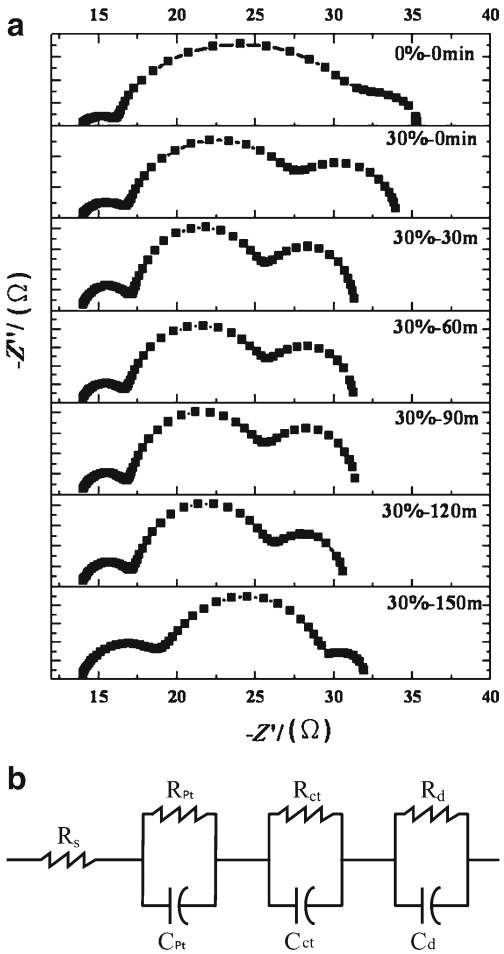

Fig. 3 **a** The Nyquist plots from EIS for DSSC cells with TiO_2 working electrodes fabricated by using (*a*) no PEG/no aggregation, and 30 % PEG loading with various isothermal heating time: (*b*) 0 min, (*c*) 30 min, (*d*) 60 min, (*e*) 90 min, (*f*) 120 min, and (*g*) 150 min. **b** The equivalent circuit for the DSSC

Table 2 Photovoltaic properties (J_{sc}, V_{oc}, FF, and η) for aragose gel electrolyte-based DSSCs using TiO_2 working electrodes using 30 % PEG under different heating time at 100 °C

Sample properties	0%—0 min	30 %—0 min	30 %—30 min	30 %—60 min	30 %—90 min	30 %—120 min	30 %—150 min
Surface area (m^2 g^{-1})	50.15	49.42	48.61	48.90	49.66	49.73	49.98
Porosity (%)	52.35	52.24	52.91	53.99	54.50	53.38	53.50
V_{oc} (V)	0.80	0.74	0.74	0.75	0.73	0.74	0.68
J_{sc} (mA cm^{-2})	10.39	13.29	14.18	14.32	14.57	13.89	11.36
FF	0.71	0.66	0.69	0.69	0.68	0.68	0.65
η (%)	5.89	6.54	7.18	7.43	7.28	7.04	4.98

between the PEG and the TiO_2 is weaker, so the highly mobile PEG molecules aggregate and collide with the TiO_2 particles, which leads to larger pores after sintering at 400 °C. When the heating time is increased to 60 min, the peak pore size continues to increase to 34–35 nm and larger pores >50 nm appear. After a longer PEG aggregation time of 120 min, larger mesopores remain and there is a peak pore size of ~32 nm, with less percentage. Up to 120 min, the TiO_2 film thickness remains at ~10 μm, with little shrinkage. These results indicate that increased heating time results in the formation of larger pores and the pore size distribution is increased because of increased PEG aggregation, due to the enhanced diffusivity of PEG at a reduced viscosity. As heating time is increased to 150 min, the approximately 32-nm pore size peak disappears and there is a narrow distribution, as seen in Fig. 3g. The decrease in the pore size distribution is attributed to the collapse of the TiO_2 film (from 10 to ~6 μm), after a heating time of 150 min.

The pore properties, such as the surface area and the porosity of the TiO_2 films prepared using a 30 % PEG loading and various isothermal heating times, are summarized in Table 2. The surface area and the porosity are virtually unchanged at approximately 49–50 m^2 g^{-1} and 53.0–54.5 %, respectively. It is seen that TiO_2 films with different pore size distributions but similar surface area are produced by using a simple heating step at 100 °C for various durations. The TiO_2 films prepared by this method provide more defined conditions for the determination of the effect of the pore size distribution in TiO_2 films on the performance of DSSCs.

The *I–V* results for an agarose gel electrolyte-based DSSC with TiO_2 films of various pore morphologies, prepared using 30 % PEG and different isothermal heating time, i.e., aggregation time, under AM 1.5, 1 sun (100 mW cm^{-2}) solar simulator illumination, are summarized in Table 2. Adding PEG into TiO_2 film and directly sintering at 400 °C results in an improvement in conversion efficiency (from 5.89 to 6.54 %) and J_{sc} (from 10.39 to 13.29 mA cm^{-2}), but a reduction in V_{oc} from 0.80 to 0.74 V. Increasing the aggregation time from 0 to 30 min results in further improvements to conversion efficiency and the J_{sc} value, to 7.18 % and 14.18 mA cm^{-2}, respectively. The form factor is increased to 0.69, but the V_{oc} value remains unchanged. An increase in the isothermal heating time to 90 min results in an improvement in the conversion efficiency of DSSCs, while the V_{oc}, *FF*, and J_{sc} values are relatively unchanged. An isothermal heating time of 120 min or more results in a decrease in the efficiency to a mere 4.98 % for a 150-min treatment time, as evidenced by the decreasing J_{sc}, V_{oc}, and *FF* values. The best performance for a DSSC is 7.43 %, for a 60-min aggregation time, which represents a 13.6 and 26.1 % improvement over the absence of aggregation (30 % PEG) and no addition of PEG, respectively. Since the surface areas of these TiO_2 films are approximately equal, these results indicate that the pore size and distribution both play a critical role in controlling DSSC performance. The dye loadings in various TiO_2 films are determined by desorption of the dye from the dyed TiO_2 after immersing in NaOH aqueous solution. This indicated that the adsorption of the TiO_2 films under different isothermal time was close and the TiO_2 film without isothermal treating owns more dye molecules due to the a little bit higher surface area than the others (Appendix 3). This does not bay the trend of the efficiency.

To determine the effect of the pore size distribution of the TiO_2 film on DSSC performance, the electron transport in the

Table 3 R_{Pt}, R_{ct}, and R_d resistances obtained from Nyquist plots for gel electrolyte-based DSSCs using TiO_2 films using 30 % PEG under different heating time at 100 °C

	0 %—0 min	30 %—0 min	30 %—30 min	30 %—60 min	30 %—90 min	30 %—120 min	30 %—150 min
R_{pt} (Ω)	2.44	3.18	3.34	2.94	3.10	3.42	5.35
R_{ct} (Ω)	15.11	10.64	8.51	9.01	8.80	8.94	10.52
R_d (Ω)	3.98	6.33	5.65	5.44	5.74	4.49	2.28

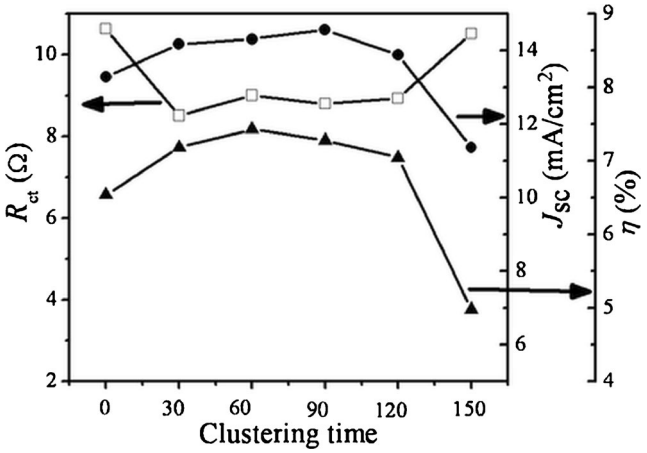

Fig. 4 The η, J_{sc}, and R_{ct} of aragose gel electrolyte-based DSSCs using TiO_2 working electrodes prepared by using 30 % PEG and under different isothermal heating time at 100 °C

TiO_2/dye/electrolyte interface and the electron diffusion within the electrolyte were examined using electrochemical impedance spectroscopy (EIS). Figure 3a, b shows the Nyquist plots and the equivalent circuit for the agarose gel electrolyte-based DSSCs with a TiO_2 electrode of various pore morphologies, with a 30 % PEG loading and using an intermediate heating step, as illustrated in Fig. 2. C_{pt}, C_{ct}, and C_d are the interface capacitances of the DSSC. The series resistance (R_s) is related to the sheet resistance of the FTO and the resistance in electrolyte and the TiO_2 film, the resistance (R_{Pt}) is related to the charge transfer at the platinum counter electrode, the resistance (R_{ct}) is related to the electron transport in the TiO_2/dye/electrolyte interface, while the resistance (R_d) is related to the Nernst diffusion within the electrolyte at low frequency. The corresponding values for the resistances, R_{Pt}, R_{ct}, and R_d, derived from the Nyquist plots, are summarized in Table 3. For 0 % PEG/no aggregation, three semicircles, relating to the R_{Pt}, R_{ct}, and R_d values for a typical DSSC, are seen in Fig. 3a. When 30 % PEG is added, the absolute value of the second semicircle in the x-direction (R_{ct}) decreases significantly from 15.11 to 10.64 Ω but R_d increases slightly and R_{pt} remains relatively unchanged. These results indicate that the charge transfer impedance at the TiO_2/dye/electrolyte interface is reduced, but charge recombination is slightly increased. As the heating time is increased from 0 to 120 min, R_{ct} decreases from 10.6 to ~9.0Ω, which is attributed to a larger pore size and distribution. When the heating time is further increased to 150 min, the value of R_{ct} increases, presumably due to the slightly reduced pore size/distribution that results from the film collapse, as shown in Fig. 2.

The porous TiO_2 electrode with no PEG addition provides narrower pathways for electrolytic diffusion into the inner TiO_2 layer, which results in a higher value for R_{ct} and a lower value for J_{sc}. When 30 % PEG is added into the TiO_2 and there is an additional isothermal heating step to enable PEG aggregation, the larger pores in TiO_2-working anode provide a wider pathway for electrolytic diffusion. This leads to faster charge transport, as evidenced by the lower value for R_{ct}, i.e., there is better contact at the interface of the TiO_2/dye/electrolyte, but there is a slight increase in the value of R_d, i.e., charge recombination. Therefore, a decreased resistance at the interface of the TiO_2/dye/electrolyte enhances the photocurrent (J_{sc}). As the aggregation time is increased to 150 min, the porous TiO_2 film collapses and there is a reduction on the pore size/distribution, which inhibits the diffusion of the electrolyte and results in an increase in the value of R_{ct} and a lower J_{sc} value.

Based on the pore morphology and conversion efficiency, the PEG aggregation process with an isothermal heating step at 100 °C effectively increases the pore sizes/distribution of the TiO_2 films, which results in an increase in the efficiency, for an aggregation time of less than 120 min, as shown in Fig. 4. The best DSSC performance is obtained by using TiO_2 film with a 60-min aggregation treatment. Impedance analysis, using EIS, shows that the enhanced efficiency is attributable to a reduction in the value of R_{ct}, i.e., the resistance at the interface between the electrolyte and the TiO_2 and the improvement in the value of J_{sc} are due to enhanced diffusion in the TiO_2 layer with a larger pore size/distribution.

Conclusions

This study develops a simple method to control the pore size distribution in the TiO_2 layer, using polyethylene glycol (PEG), while maintaining a similar surface area and porosity. Meanwhile, the morphologies of the TiO_2 films were only slightly modulated, whose changes were not easily detected by SEM but BET and EIS.

Impedance analysis, using EIS, shows that the enhanced efficiency is attributable to a reduction in the value of R_{ct}, i.e., the resistance at the interface between the electrolyte and the TiO_2 and the improvement in the value of J_{sc} is due to enhanced diffusion in the TiO_2 layer with a larger pore size/distribution. For the optimized TiO_2 film with larger pores/distribution (30 % PEG loading, 100 °C/60 min), an efficiency of 7.43 % is achieved for an agarose gel electrolyte-based DSSC, which represents a 26.1 % improvement over TiO_2 without PEG addition. By minimizing the variation of the TiO_2 (surface area and porosity), larger pores modify the interface between the electrolyte and the TiO_2 and represent a 13.6 % improvement (6.54–7.43 %) of efficiency.

Acknowledgments The authors thank the National Science Council of Taiwan for the financial support under Grant Nos: NSC101-2112-E-009-126-MY2 and NSC 102-3113-E-007-001-.

References

1. O'Regan B, Grätzel M (1991) A low-cost, high-efficiency solar cell based on dye-sensitized colloidal TiO_2 films. Nature 353:737–740
2. Yella A, Lee H-W, Tsao HN, Yi C, Chandiran AK, Nazeeruddin MK, Diau EW-G, Yeh C-Y, Zakeeruddin SM, Grätzel M (2011) Porphyrin-sensitized solar cells with cobalt (II/III)–based redox electrolyte exceed 12 percent efficiency. Science 334:629–634
3. He W, Qiu J, Choi S-K, Kim W-D, Lee J-H, Kim Y-D, Kim S-H, Kim H-K, Hwang Y-H (2011) Improved conversion efficiency of dye-sensitized solar cell based on the porous anodic TiO_2 nanotubes. Curr Appl Phys 11(3, Supplement):S320–S323
4. Lin L-Y, Yeh M-H, Lee C-P, Chen Y-H, Vittal R, Ho K-C (2011) Metal-based flexible TiO_2 photoanode with titanium oxide nanotubes as the underlayer for enhancement of performance of a dye-sensitized solar cell. Electrochim Acta 57:270–276
5. Wang Z-S, Kawauchi H, Kashima T, Arakawa H (2004) Significant influence of TiO_2 photoelectrode morphology on the energy conversion efficiency of N719 dye-sensitized solar cell. Coord Chem Rev 248:1381–1389
6. Katoh R, Fuke N, Furube A, Koide N (2010) Effect of dye coverage on photo-induced electron injection efficiency in N719-sensitized nanocrystalline TiO_2 films. Chem Phys Lett 489:202–206
7. Mikroyannidis JA, Charalambidis G, Coutsolelos AG, Balraju P, Sharma GD (2011) Novel zinc porphyrin with phenylenevinylene meso-substituents: synthesis and application in dye-sensitized solar cells. J Power Sources 196:6622–6628
8. Lee KE, Gomez MA, Elouatik S, Demopoulos GP (2010) Further understanding of the adsorption mechanism of N719 sensitizer on anatase TiO2 films for DSSC applications using vibrational spectroscopy and confocal raman imaging. Langmuir 26:9575–9583
9. Yanagida S, Yu Y, Manseki K (2009) Iodine/iodide-free dye-sensitized solar cells. Acc Chem Res 42:1827–1838
10. Benedetti JE, Gonçalves AD, Formiga ALB, De Paoli M-A, Li X, Durrant JR, Nogueira AF (2010) A polymer gel electrolyte composed of a poly(ethylene oxide) copolymer and the influence of its composition on the dynamics and performance of dye-sensitized solar cells. J Power Sources 195:1246–1255
11. Lee SU, Choi WS, Hong B (2010) A comparative study of dye-sensitized solar cells added carbon nanotubes to electrolyte and counter electrodes. Sol Energy Mater Sol Cells 94:680–685
12. Yang C-C, Zhang HQ, Zheng YR (2011) DSSC with a novel Pt counter electrodes using pulsed electroplating techniques. Curr Appl Phys 11(1, Supplement):S147–S153
13. Tsai C-H, Hsu S-Y, Lu C-Y, Tsai Y-T, Huang T-W, Chen Y-F, Jhang Y-H, Wu C-C (2012) Influences of textures in Pt counter electrode on characteristics of dye-sensitized solar cells. Org Electron 13:199–205
14. Weisspfennig CT, Hollman DJ, Menelaou C, Stranks SD, Joyce HJ, Johnston MB, Snaith HJ, Herz LM (2014) Dependence of dye regeneration and charge collection on the pore-filling fraction in solid-state dye-sensitized solar cells. Adv Funct Mater 24:668–677
15. Wang B, Chang S, Lee LTL, Zheng S, Wong KY, Li Q, Xiao X, Chen T (2013) Improving pore filling of gel electrolyte and charge transport in photoanode for high-efficiency quasi-solid-state dye-sensitized solar cells. ACS Appl Mater Interfaces 5:8289–8293
16. Chen W, Qiu Y, Yan K, Yang S (2011) Surfactant directed self-assembly of size-tunable mesoporous titanium dioxide microspheres and their application in quasi-solid state dye-sensitized solar cells. J Power Sources 196:10806–10816
17. Yu Z, Carter RN, Zhang J (2012) Measurements of pore size distribution, porosity, effective oxygen diffusivity, and tortuosity of PEM fuel cell electrodes. Fuel Cells 12:557–565
18. Franco AA, Xue KH (2013) Carbon-based electrodes for lithium air batteries: scientific and technological challenges from a modeling perspective. ECS J Solid State Sci Technol 2:M3084–M3100
19. Ni M, Leung MKH, Leung DYC, Sumathy K (2006) An analytical study of the porosity effect on dye-sensitized solar cell performance. Sol Energy Mater Sol Cells 90:1331–1344
20. Kim H-S, Ko S-B, Jang I-H, Park N-G (2011) Improvement of mass transport of the [Co(bpy)3]II/III redox couple by controlling nanostructure of TiO_2 films in dye-sensitized solar cells. Chem Commun 47:12637–12639
21. Lan Z, Wu J, Lin J, Huang M (2010) PF127 aided preparation of super-porous TiO_2 film used in highly efficient quasi-solid-state dye-sensitized solar cell. J Mater Sci Mater Electron 21:1000–1004
22. Lee K-M, Hsu C-Y, Chiu W-H, Tsui M-C, Tung Y-L, Tsai S-Y, Ho K-C (2009) Dye-sensitized solar cells with a micro-porous TiO_2 electrode and gel polymer electrolytes prepared by in situ cross-link reaction. Sol Energy Mater Sol Cells 93:2003–2007
23. Saito Y, Kambe S, Kitamura T, Wada Y, Yanagida S (2004) Morphology control of mesoporous TiO_2 nanocrystalline films for performance of dye-sensitized solar cells. Sol Energy Mater Sol Cells 83:1–13
24. Lee K-M, Suryanarayanan V, Ho K-C (2009) Influences of different TiO_2 morphologies and solvents on the photovoltaic performance of dye-sensitized solar cells. J Power Sources 188:635–641
25. Kim YJ, Lee MH, Kim HJ, Lim G, Choi YS, Park N-G, Kim K, Lee WI (2009) Formation of highly efficient dye-sensitized solar cells by hierarchical pore generation with nanoporous TiO_2 spheres. Adv Mater 21:3668–3673
26. Fei Z, Kuang D, Zhao D, Klein C, Ang WH, Zakeeruddin SM, Gratzel M, Dyson PJ (2006) A supercooled imidazolium iodide ionic liquid as a low-viscosity electrolyte for dye-sensitized solar cells. Inorg Chem 45:10407–10409
27. Hsu H-L, Hsu W-T, Leu J (2011) Effects of evironmentally benign solvents in the agarose gel electrolytes on dye-sensitized solar cells. Electrochim Acta 56:5904–5909
28. Hsu H-L, Tien C-F, Yang Y-T, Leu J (2013) Dye-sensitized solar cells based on agarose gel electrolytes using allylimidazolium iodides and environmentally benign solvents. Electrochim Acta 91:208–213
29. Dombrowski RJ, Hyduke DR, Lastoskie CM (2000) Pore size analysis of activated carbons from argon and nitrogen porosimetry using density functional theory. Langmuir 16:5041–5050
30. Orita A, Kamijima K, Yoshida M (2010) Allyl-functionalized ionic liquids as electrolytes for electric double-layer capacitors. J Power Sources 195:7471–7479
31. Zhou C-H, Zhao X-Z, Yang B-C, Zhang D, Li Z-Y, Zhou K-C (2012) Effect of poly (ethylene glycol) on coarsening dynamics of titanium dioxide nanocrystallites in hydrothermal reaction and the application in dye sensitized solar cells. J Colloid Interface Sci 374:9–17
32. Long TC, Saleh N, Tilton RD, Lowry GV, Veronesi B (2006) Titanium dioxide (P25) produces reactive oxygen species in immortalized brain microglia (BV2): implications for nanoparticle neurotoxicity. Environ Sci Technol 40:4346–4352
33. Chen Y-H, Jeng U-S, Leu J (2011) Effect of curing on the porogen size in the low-k MSQ/SBS hybrid films. J Electrochem Soc 158: G52–G57
34. Halpin-Healy T, Zhang Y-C (1995) Kinetic roughening phenomena, stochastic growth, directed polymers and all that. Aspects of multidisciplinary statistical mechanics. Phys Rep 254:215–414